HIGH PRODUCTIVITY VACUUM BLASTING SYSTEM

William S. McPhee wsmcphee@home.com (703) 566-0942
LTC Teletrak, Inc. (an Advanced Environmental Systems Company)
P.O. Box 25432, Alexandria, VA, 22313

Dr. M. A. Ebadian ebadian@eng.fiu.edu (305) 348-4238
Hemispheric Center for Environmental Technology
Florida International University
10555 West Flagler Street, Suite 2100
Miami, FL 33174

ABSTRACT

The objective of this project is to improve the productivity and lower the expense of existing vacuum blasting, an already proven technology used to remove radioactive contamination, PCBs, and lead-based paint. The technology minimizes waste and provides worker protection by continuously recycling the blasting material and containing the dust during the decontamination process. The development work will increase the cleaning rate and provide safe and cost-effective decontamination of the DOE sites.

Improvements to the existing (or baseline) vacuum blasting technology, were proposed by implementing an innovative design of certain components, namely, the nozzle, blasthead, and dust separator. The project includes numerical analysis, production of prototypes to test in a lab environment, and ultimate integration with LTC's Sealed Waste Transfer System (SWATS™) and LTC's Vacuum Blasting Machines and the investigation of their performance in the field. See a x-section of a machine below.

Research both from the open blasting industry and vacuum blasting has shown that the performance of the nozzle can be improved in three ways: 1) run at the design nozzle pressure or above; 2) use the smallest feasible abrasive grit size; 3) use an improved blasting nozzle. Among these three, the redesign of the nozzle alone offers an estimated 80 percent increase in efficiency. Work done recently with rectangular shaped nozzles has achieved an order of magnitude increase in the overall performance. The second component to be considered is the dust separator. Fine steel grit particles are useful for improving the cleaning production rate. However, such fine particles are easily entrained by the fine particles and dust cleaned from the decontaminated surfaces. This decreases the overall efficiency of the system. A newly designed high performance separator has been designed and tested. The new blast head incorporates the sensors for triggering shut-down when the blast head is taken away from the cleaning surface. Sensors are needed to ensure neither "under or over" cleaning of a given surface area that result in loss of production rates, and to perform real-time characterization to determine the effectiveness of decontamination.

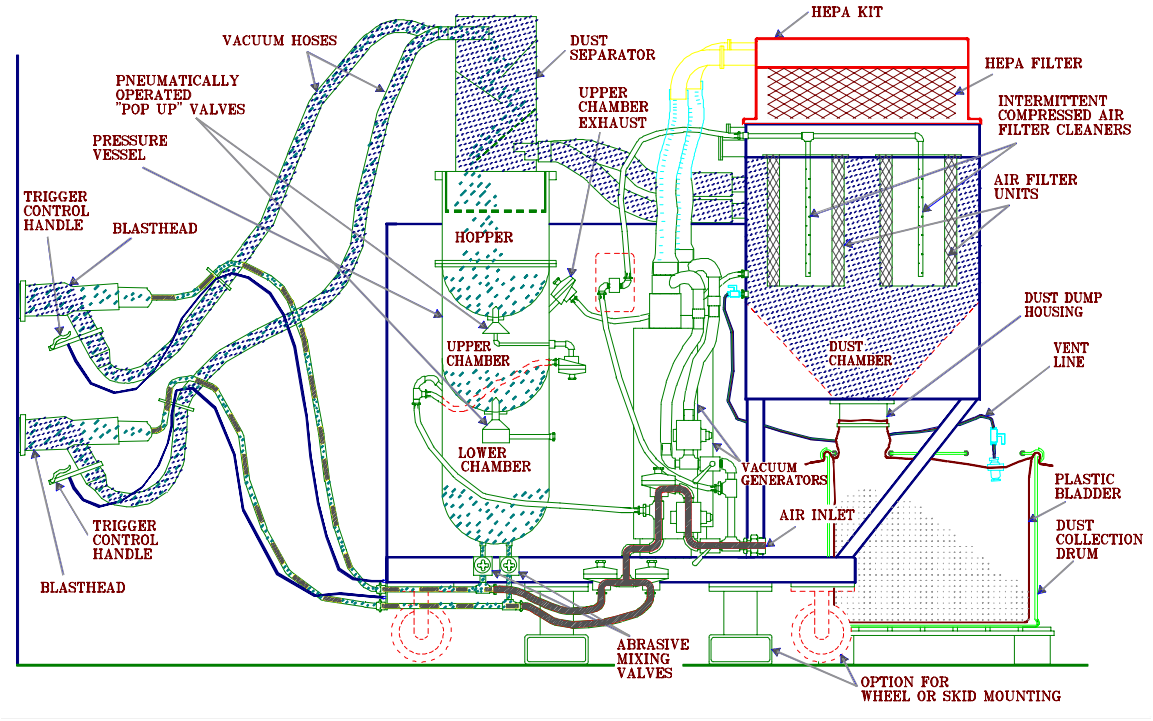

VACUUM BLASTING MACHINE Model LTC 1072
X-Section Including LTC's Sealed Waste Transfer System (SWATS™)

INTRODUCTION

The work focuses on redesigning and improving existing vacuum blasting technology including blast head nozzles, ergonomic handling of the blast head by reducing its weight; brush-ring design, vacuum level regulator, efficiency of the dust separator, and operational control sensors. The redesign is expected to enhance the productivity and economy of the vacuum blasting system by at least 50 percent over current vacuum blasting systems.

There are three phases in the project. Phase I now completed, focused on developing and testing mathematical models. Phase II consists of pre-prototype design and fabrication and pre-prototype unit testing. Phase III consists of prototype design and field verification testing.

In order to meet the need of phase I, we first developed mathematical model and related code to simulate the entire process numerically. Second, based on the modeling data, we designed, manufactured, and finally tested an innovative rectangular nozzle and a new centrifugal separator. The experimental results agreed with the numerical estimated data with a deviation within ±10%, thus proving the mathematical model and the model test successful.

PART 1. NUMERICAL MODELING

1.1 Two-phase mathematical model

The air-particle two-phase model, incorporating some existing models, has been developed for simulating two-phase flow in the key components and the entire vacuum blasting system. The calculations were performed for the blasting nozzle, separator, and blasthead/wind curtain.

For the continues phase (air) flow in the entire vacuum blasting system, the fully three-dimensional compressible Navier-Stoke equations were used to simulate the continues phase (air) flow in blasting nozzle; the two-dimensional incompressible Navier-Stokes equations were used to simulate the air flow in the existing separator and wind curtain; the three-dimensional incompressible Navier-Stokes equations were used to simulate the air flow in the centrifugal separator.

The standard κ~ε model was adopted in this study. This turbulence model contains the transprot model equation considering the turbulent kinetic energy (κ) and its dissipation rate (ε). The κ equation was derived from the exact equation, while the ε equation was obtained using physical reasoning and bears little resemblance to its mathematically exact conterpart.

The discrete phase (particles) was simulated in a Lagrangian frame of reference. The discrete phase consisted of spherical particles dispersed in the continuous phase(air). The trajectory of the discrete phase particle was predicted by integrating the force balance on the particle, which was written in a Lagrangian reference frame. This force balance equated the particle inertia with the forces acting on the particle.

The dispersion of particles due to turbulence in the fluid phase is modeled using the stochastic discrete-particle approach. In this approach, the turbulent dispersion of particles is predicted by integrating the trajectory equations for individual particles, using the instantaneous fluid velocity along the particle path during the integration. Computing the trajectory in this manner for a

sufficient number of representative particles may account for the random effects of turbulence on the particle dispersion. In this study, the Discrete Random Walk (DRW) model is used. In this model, the fluctuation velocity components are discrete piecewise constant functions of time. Their random values are kept constant over an interval of time give by the characteristic.

There are two sets of boundary conditions. The first one is for the continuous phase (air); the second is for the discrete phase (particle).

For the continuous phase (air), a non-slip boundary condition was imposed on the wall. The total pressure, temperature, and static pressure were known at the nozzle entrance. At the nozzle exit plane, all flow quantities were extrapolated from the two neighboring interior planes upstream of the exit plane. For separator and blasthead/wind curtain, the velocity inlet and pressure outlet boundary conditions were imposed on inlet and outlet plane.

For the discrete phase (particle), the following discrete phase boundary conditions were adopted:

- Inlet: "Escape" , which indicates the particle as having "escaped" when it encounters the boundary in question, thereby terminating trajectory calculations.
- Outlet: "Escape"
- Wall: "Reflect," a coefficient of restitution equal to 1.0, which indicates the rebound of the particle from the boundary in question with a change in its momentum being defined by the coefficient of restitution. A coefficient of restitution equal to 1.0 implied that the particle retained all of its normal momentum after the rebound (an elastic collision).

Two kinds of standard steel grits were adapted in this study: G40 with a particle size of 820 μm, and G80 with a particle size of 300 μm. Both have the specific gravity of 7.0 g/cm^3.

1.2 Numerical results and discussion (blasting nozzles)

1.2.1 Numerical results on the existing round nozzle

The calculations were performed with the fully three-dimensional model. The particle concentration distribution at the exit plane was obtained. Figure 1 shows the grid generation of the existing round nozzle with a throat diameter of ¼ inch. Several cases for different inlet pressure have been run. When the nozzle inlet pressure was 100 Psi, the statistic average particle velocities on the exit plane of the nozzle were just 45m/s for G40 steel grit and 70 m/s for G80 steel grit, probably because the nozzle is too short to provide enough residence time for the steel grit in the nozzle. This is one of the major disadvantages. The particle distribution at the exit plane of the nozzle is shown in Figure 2. When blasting, the steel particles were too concentrated, resulting in a narrow particle beam with a diameter of 0.46 inch (in a total circular area with a diameter of 0.72 inch). This is the second major disadvantage.

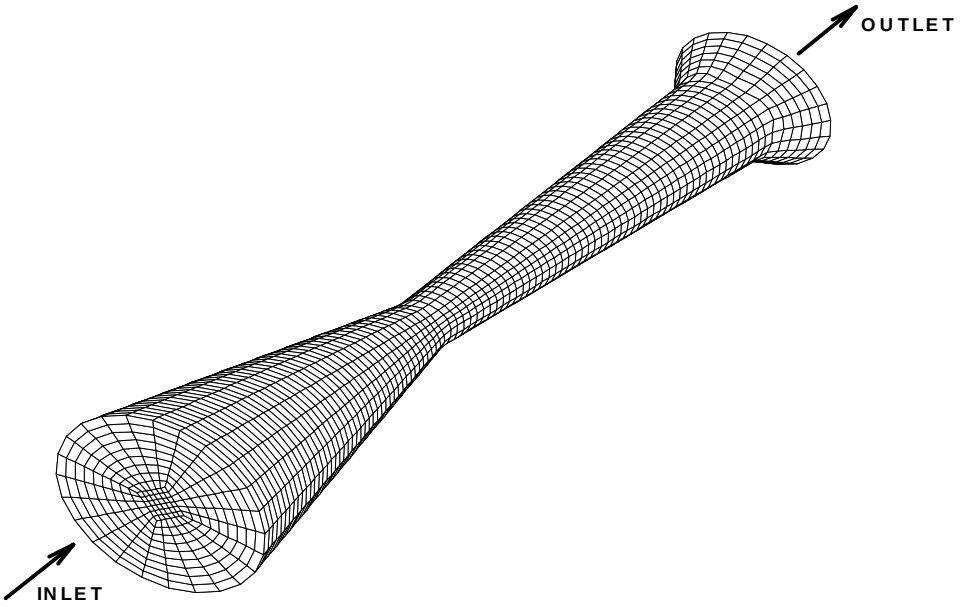

Figure 1. Multi-block structured grid of existing round nozzle (the total cells are about 35,000)

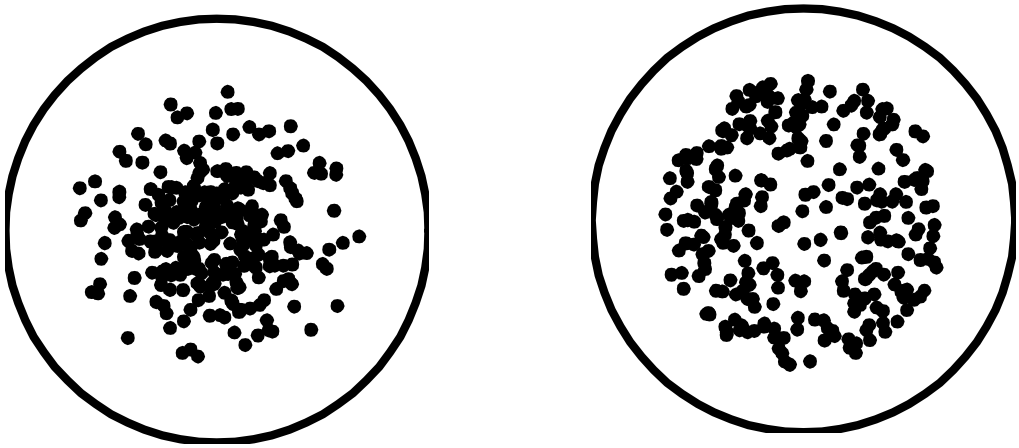

.

G40 **G80**

Figure 2. Particles distribution at exit plane of the existing round nozzle.

1.2.2 Numerical results on the new rectangular nozzle

There are two major disadvantages of the existing round nozzle. One is lower particle velocity, and the other is the concentrated particle distribution. The two disadvantages greatly limit the blasthead cleaning rate. The main reasons are that the length of the round nozzle is too short (3.86 inch) and the structure of the round nozzle is not optimum. Although the blasthead cleaning rate

can be increased by increasing the length of the existing round nozzle, theoretically there still exists other substantial disadvantages in the configuration of the round nozzle.

In this project, the new rectangular nozzle was proposed to overcome the disadvantages of the existing round nozzle. The new rectangular nozzle also provided convenient for redesigning the entire vacuum blasting system which will be discussed later. The geometry and grid system of the new rectangular nozzle is shown in Figure 3. Two kinds of rectangular nozzles with 1/4 and 3/8 inch equivalent throat diameters were calculated for different lengths. The objective is to verify how the nozzle length affects the velocity and particle distribution and choose a suitable length. The theory is that increasing the nozzle length results in long resident time of the particles in the nozzle and increases the particle velocity. These cases are obtained with the same conditions. Figure 4 shows the particle velocity at nozzle exit plane versus nozzle divergent length for ¼ inch equivalent throat diameter. Similar trends for both G-40 and G-80 particle grit were observed. Figure 5 shows the results for 3/8 inch equivalent throat diameter. The particle velocities are higher than those with ¼ inch equivalent diameter.

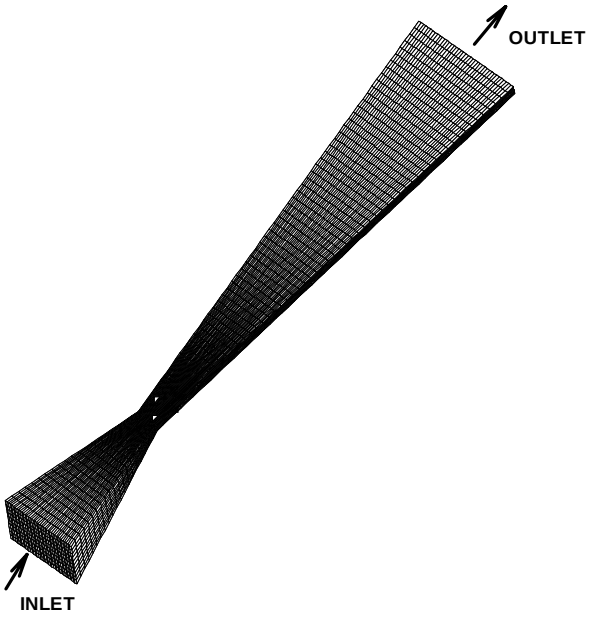

Figure 3. Structured grid of the rectangular nozzle (total cells approx 35,000)

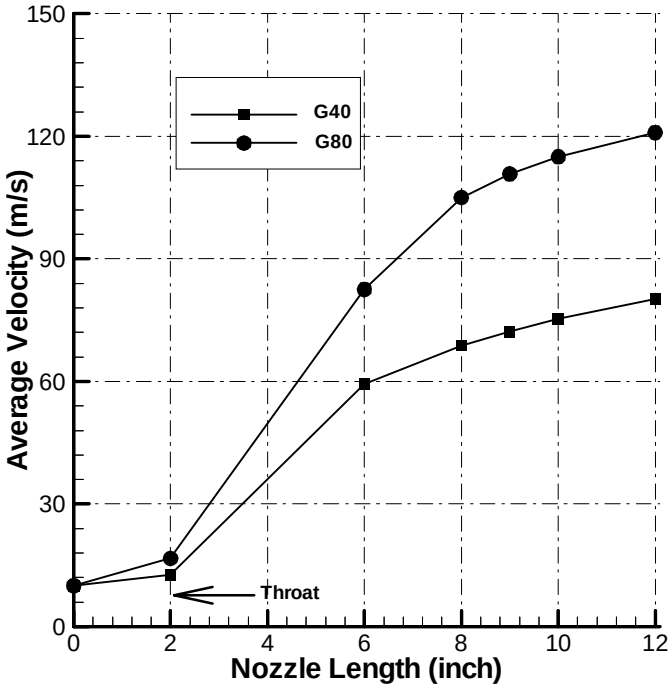

Figure 4. Particle velocities on the exit plane of the rectangular nozzle (1/4" equivalent throat diameter)

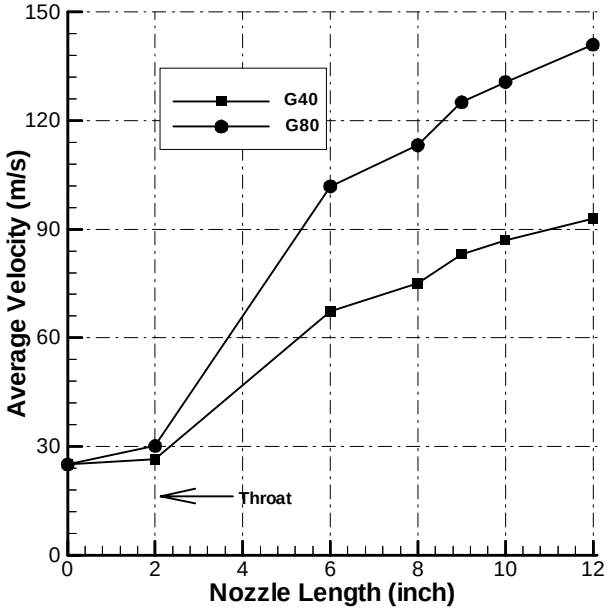

Figure 5. Particle velocities on the exit plane of the rectangular nozzle (3/8 inch equivalent throat diameter).

Based on the above numerical results and from the practical application point of view, the optimal geometry parameters of the rectangular nozzle were determined. Four rectangular nozzles with ¼ and 3/8 inch equivalent throat diameter, and each with a different flow passage thickness, were chosen for further research so as to optimize the configuration.

With ¼ inch hydrodynamic diameter, two nozzles with a 1/8 inch and 3/16 inch flow passage thickness, named nozzle #1 and nozzle #2 respectively, were calculated. The difference between these two nozzles just existed in the flow passage thickness. Table 1 illustrated the particle velocities for two nozzles with grit G40 and G80. It seems that the thickness does not affect the particle velocity more, and the velocities with fine grit G80 were always higher than those with coarse grit G40. Compared with the numerical results of the existing round nozzle at the same conditions, the statistic average particle velocities at the exit plane of the nozzle were increased more than 50%. Figure 6 shows the particle distribution at the exit plane. It is better for the nozzle with 3/16 inch flow passage thickness. The particles nearly cover the whole cross-section of the exit plane.

Table 1. The average particle velocities at exit plane of the rectangular nozzle

	Nozzle #1	Nozzle #2
Particle: G40	67m/s	62m/s
Particle: G80	104m/s	100 m/s

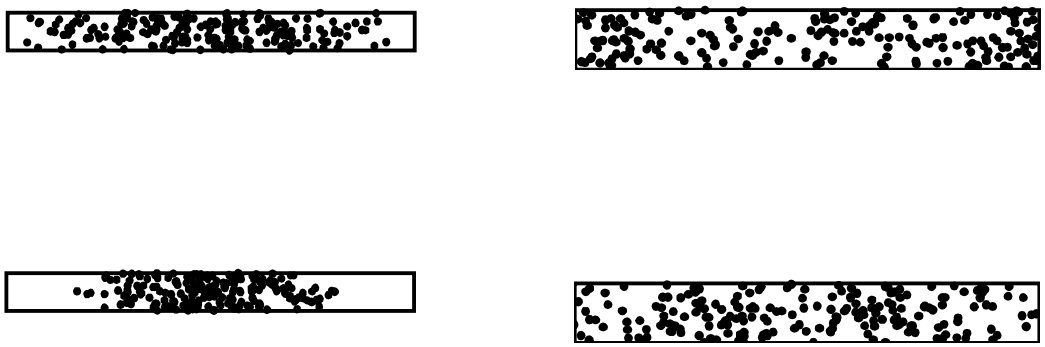

(a) Nozzle #1, Top-G40, Bottom –G80 (b) Nozzle #2, Top-G40, Bottom –G80

Figure 6. Particles distribution at exit plane of the nozzle.

Similarly, two nozzles for 3/8 inch hydrodynamic throat diameters, but with a 3/16 and 4/16 inch flow passage thickness were calculated. The numerical results revealed same conclusion as that of the rectangular nozzle with ¼ inch hydrodynamic diameter. Therefore, the new designed rectangular nozzle can increase the particles velocity more than 50% than that of the existing round nozzle, and the particle distribution on the exit plane are more reasonable. All of the above results were obtained at the ideal boundary condition: the inlet pressure was fixed at 100 psi, the wall of the nozzle was smooth, and the particles were considered as spherical, etc.

1.3 Numerical results and discussion (dust separators)

1.3.1 Numerical results of the existing separator

In order to determine the performance of the existing separator, numerical simulations have been carried out. Numerical results showed that the air flow is concentrated in the center of the cylinders. It is estimated that the relative concentrated air flow may bring some particles out of the separator during the separating process. The calculated results of the separation efficiency can prove the above conclusion. Under this condition, the separation efficiency is about 90% for the steel grit G40, but it is just about 27% for steel grit G80.

1.3.2 Numerical results of the new centrifugal separator

Numerical modeling was performed to investigate the air flow field, particle trajectory, and collection efficiency. The inlet boundary condition is set to 10 m/s for the average air velocity. Fully three-dimensional calculations are performed with incompressible flow assumption. Non-uniform, unstructured grids are chosen to discretize the entire computation domain.

The geometry and grid system of the new centrifugal separator is shown in Figure 7, and almost 100,000 cells are used to discretize the computation domain. The numerical results of air fields showed that the air flows down first, then turns to the exit of the separator due to the vacuum force. It is estimated that this air flow can entrain some small-sized particles out of the separator. Some large particles or heavy particles are collected in the bottom of the separator.

The numerical results also reveals that a separator's geometry can affected the separation efficiency. With the increase of separator outside diameter, the separation efficiency increases. When the efficiency reaches the maximum value, it decreases with the outside diameter. Finally, the outside diameter that can provide the best separation efficiency is chosen for the new separator's outside diameter, i.e., 6 inches.

In this case (the outside diameter is 6 inches), the calculated separation efficiency is about 70% for steel grit G80. Compared with the existing separator, the separator efficiency for steel grit G80 was almost double. Therefore, the new centrifugal separator can separate the finer grit well; of course, it can separate the coarse grit.

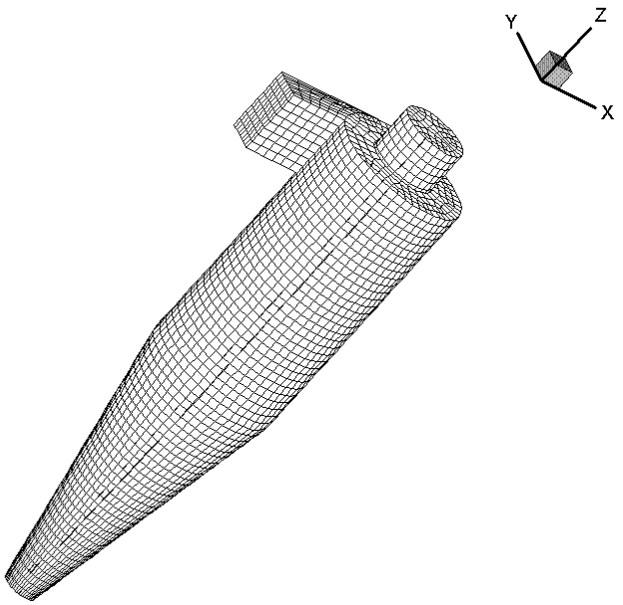

Figure 7. The grid system of the new centrifugal separator.

1.4 Numerical results and discussion (wind curtain)

The wind curtain is expected to have two functions. One is to create an air barrier to prevent the particles escaping to the atmosphere. The other is to make the blasthead float on the wall surface and balance the forces. To meet the above need, the configuration shown in Figure 8 was adopted.

Because the wall surface can not be very smooth, a gap between the wall surface and the blasthead was considered. The injected air has a fixed pressure, and the geometry has an inclined angle. The numerical modeling was performed to study the air flow field for the wind curtain. For the air injection system, the channel gap and the channel inclined angle are the main parameters. The blasthead working distance is also an important parameter.

Three channel gaps of the wind curtain, of 1/16, 1/8 inch, and 1mm, were chosen for numerical modeling. The numerical modeling was conducted for each channel gap with 30°, 45°, and 60° inclination angles. The assumed working distances are from 0.1 to 3 inch. One of the calculation cases on the air flow field in the wind curtain is shown in Figure 9. The assumed working distance effect on wind curtain efficiency, which means the statistical percentage of particles contained inside the wind curtain, at different inject pressure is shown on Figure 10. It was concluded the proposed wind curtain will be able to meet the desired need.

The lift force can also be balanced. The criteria of the optimum parameters are based on calculated results and a practical view.

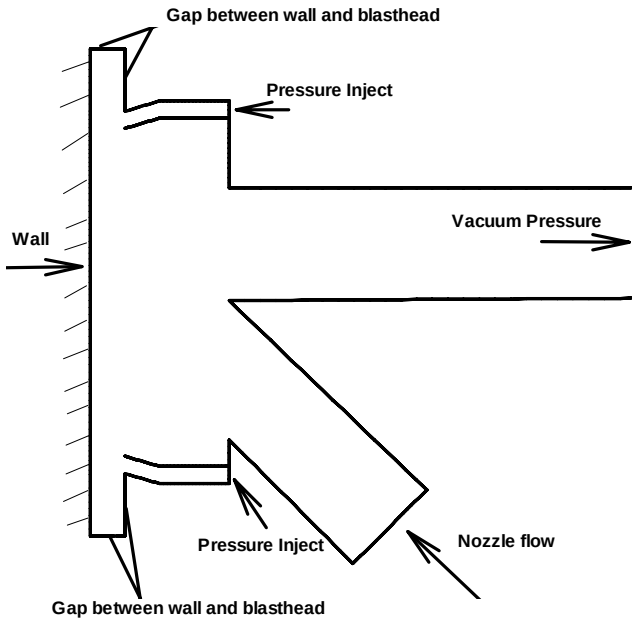

Figure 8. Proposed geometry of wind curtain.

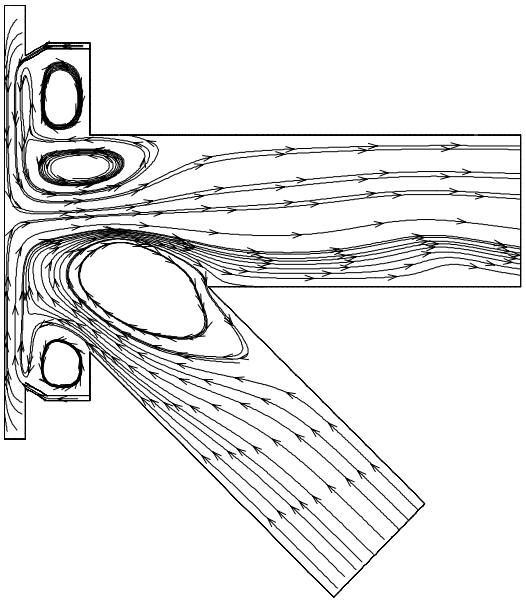

Figure 9. Air flow field on the proposed wind curtain (gap=1/16 inch, angle = 60°, working distance = 0.25 inch).

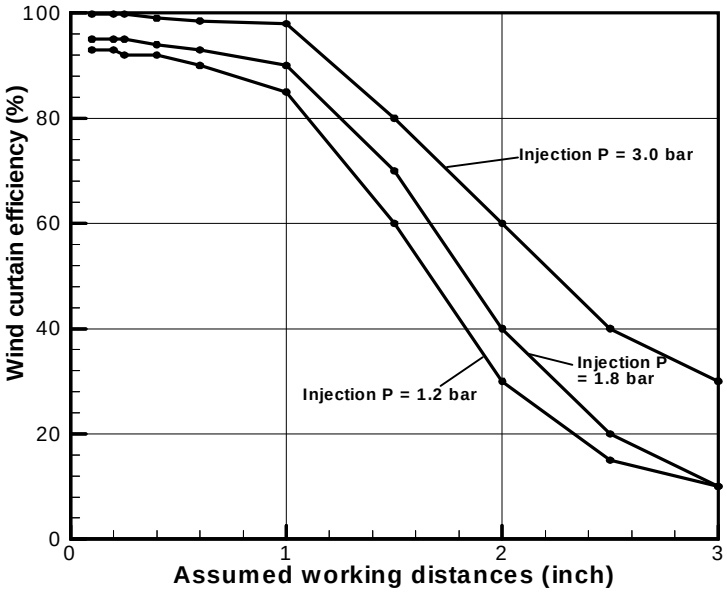

Figure 10. Assumed working distance versus the wind curtain efficiency at different injection pressure.

PART 2. DESIGN AND SELECTION OF BLASTHEAD SENSORS

2.1 Blasthead sensors

2.1.1 Radiological characterization sensor system

The concept design is complete. The system will have four major subsystems: transducers (2); transducer interface electronic modules (2); control electronic module; and operator interface module; see Figure 11.

The transducers (2) will be incorporated into the structure of the blasthead as compactly as possible to minimize the standoff distance from an adjacent perpendicular surface, Figure 12. A transducer is situated in the forward path, and a second transducer is situated in the following path of the blasthead. This arrangement allows feedback to the operator indicating degree of contamination and success at decontamination.

2.1.2 Lift-off sensor system

Two conceptual lift-off sensor system designs have been generated. The preferred design incorporates sensitive differential pressure switches/transducers to monitor the generated negative pressure within the blasthead. Any significant separation of the head from the surface will

necessarily reduce the effective vacuum. An anticipated additional beneficial effect is an incipient failure of the vacuum effluent retrieval system and will be detected. This concept is most efficient in use of space and weight, as well as superior in expected effectiveness.

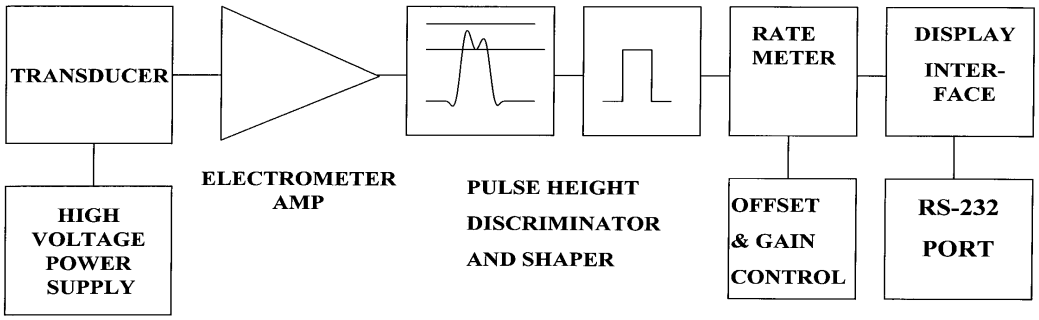

Figure 11. Radiological characterization electronics.

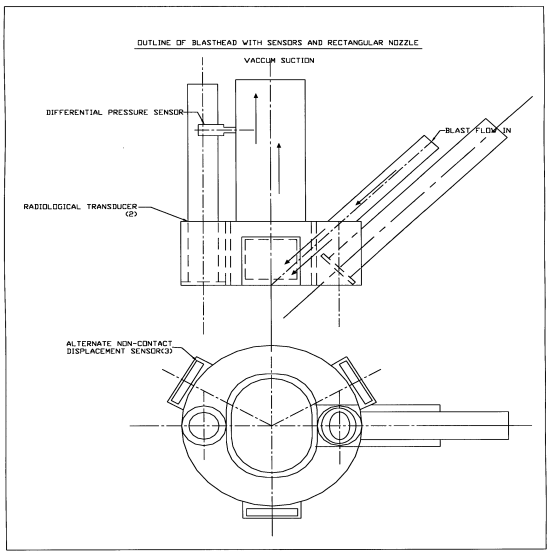

Figure 12. Arrangement of sensor components with compact blasthead chamber design.

PART 3. MODEL TEST RESULTS

The experimental results on the blasting nozzle and the new centrifugal separator, were compared with numerical modeling. A flow loop, with air-particle two-phase flow has been set up. Combined with the LTC Vacuum Blasting Machine, the facilities have been successfully running. With the Phantom High-Speed Video Camera system, the particle velocity and their concentrations are measured, for both the existing circular nozzle and the new rectangular nozzle of ¼ inch diameter. The measurements matched the numerical predictions well, with the maximum

distinction below 10.0%. A 6060P Pitot probe from ALNOR INSTRUMENT COMPANY was employed to obtain the velocity distribution. The comparison of experimental data and CFD modeling results showed that the design of the new centrifugal separator was successful.

3.1. Experimental results and their comparison with CFD modeling on the blasting nozzle

3.1.1 Description of setup

Figure 13 illustrates the layout of the experimental setup. The LTC Vacuum Blasting Machine has been used to produce the blasting air-particle two-phase flow and the vacuum pipeline will be used to recycle the steel grit.

3.1.2 Working mechanism

The air-particle two-phase mixture flows through the blasting nozzle. At the exit of the nozzle, the steel grit particles have a higher velocity. Between the blasting nozzle and the collection box, there is a rectangular glass channel ($1\times1\,\text{ft}$) with a length of 2 ft, through which the steel particles pass as a high-speed jet. The collection box collects the steel grit from the nozzle. This collection box is connected with the vacuum pipeline that is used to recycle the grit, after transporting the grit particles in the machine (see Figure 13).

3.1.3 Instruments and test sections

Three instruments are installed to measure the air flow rate, air temperature, and air pressure. The Phantom v3.0 High Speed Digetor Motion Analysis System is used to measure the steel grit velocity and the steel grit concentration in the experimental setup. The complete Phantom system includes three major components: a high-speed camera, pulsed laser source, and PIV software. This system is the combination of a high-speed imager, capturing several thousand images per second, with the short duration sheet lighting formed by pulsed laser, that allows us to create sharp, clear pictures of a cross-sectional area of the flow. Since the pulsed duration of the laser (and hence the exposure time per image) is only 30 nanoseconds, the pictures were be sharp and blur-free to facilitate the measurements. After an image is complete, the PIV software is used to do particle tracking, auto or cross-correlation.

Figure 14 illustrates the measurement mechanism of the particle velocity and concentration. The nozzle produces the high speed air-particle jet along the x coordinate. Y is the vertical coordinate. The pulsed laser creates a vertical laser sheet with very short time duration and separation. Because the environment is “dark,” the moving particles can only be captured when the laser is on. The first dot is created on the image when the first laser pulse arrives. Continuously the second dot will be produced when the second laser pulse comes. The time difference between the first and the second laser pulse is defined as the time separation. For the present measurement, the particle velocity is very high; thus, short time separation is needed. The experiments show that it is suitable to choose the time separation of 25 μs. Four laser pulses create four dots in the image, and the total time is $3\times25\,\mu\text{s}$. The following simple expression is used to calculate the particle velocity:

$$v = \frac{d \times 10^{-3}}{3 \times 25 \times 10^{-6}}$$

The units of d and v are mm and m/s, respectively.

Next is particle concentration measurement. Through data processing of the image file, two lines, lines AB and CD, can be identified to cover all particle dots in the image. Extending the two lines to the nozzle exit plane obtains the line EF, which is identified as the length of the particle coverage in y direction. For the circular nozzle, EF is the circular diameter that the particles cover at the nozzle exit plane. For the rectangular nozzle, two measurements are conducted: one with long side (EF) at horizontal position, and the other with long side (EF) at vertical position. Through data processing, the covering area of the particles at the exit plane can also be obtained.

Figure 15 showed the test set-up section for the particle velocity measurement. Two test models were used in this experiments. One is the existing round nozzle, and the other is the new rectangular nozzle with ¼ inch hydrodynamic throat diameter.

3.1.4 Experimental results and comparison with numerical modeling

Excellent image files were obtained. Figures 16 shows the particle imaging from the experimental process of one of nozzle and flow pressure tests. It showed that the particles almost fill in the rectangular nozzle blasting areas.

Table 2 Comparison of the measurement results with numerical modeling data

Nozzle	Pressure, psi	Velocity, m/s (measurements)	Velocity, m/s (CFD modeling)	Deviation
Circular nozzle	65	48.8	54	10.0%
Circular nozzle	83	58.3	64	9.8%
Rectangular	65	82.1	91	9.9%
Rectangular	82	112.0	101	10.0%

Table 2 provides a comparison of the measurements with the numerical modeling at the same conditions and the magnitude of velocity is a statistic average magnitude. As evidenced in Table 2, the deviation of the experimental results from the modeling data is within ±10%. Therefore, the model chosen for the numerical simulation was correct.

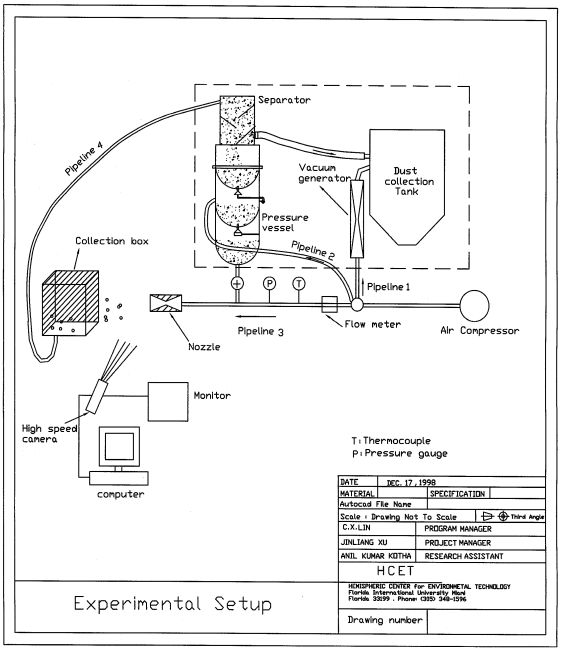

Figure 13. Experimental setup of particle velocity and concentration measurement of the blasting nozzle.

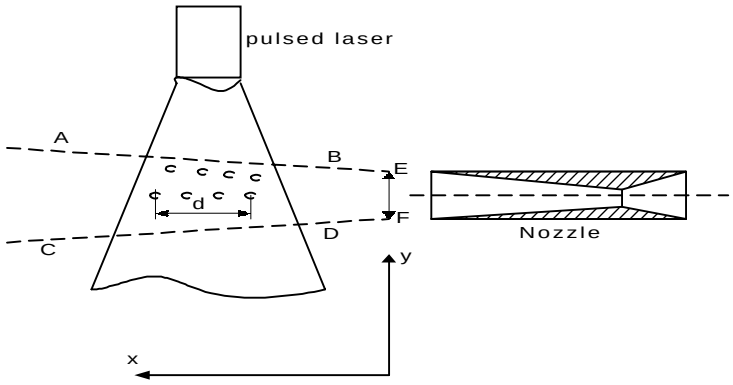

Figure 14. Measurement mechanism of the particle velocity and concentration.

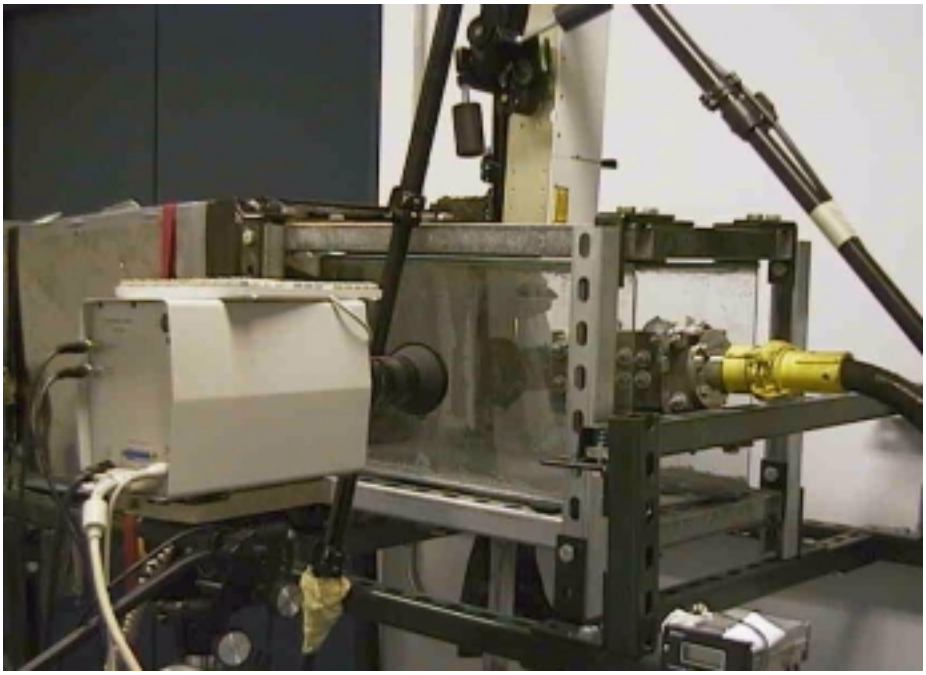

Figure 15. The test section for measuring blasting nozzle velocity and construction.

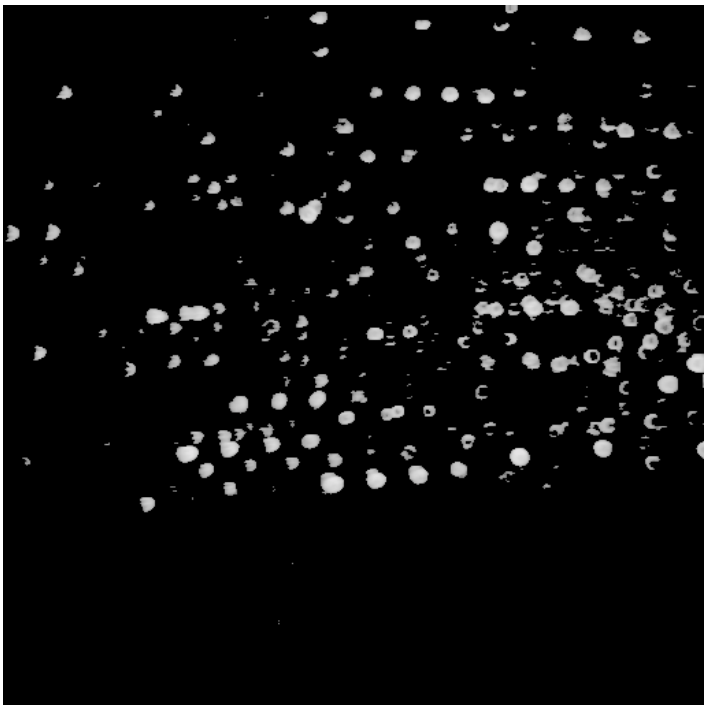

Figure 16. Particles imaging for rectangular nozzle at P =65 psi

3.2 Centrifugal separator test results

3.2.1 Efficiency test

The testing of the new separator's separation efficiency was carried out for the same working conditions as the nozzle tests. The experiment procedure was as follows.

First, the new separator was fed by two kinds of dust obtained from the existing separator. The two kinds of dust were classified as concrete dust and coating dust. Second, the new separator's dust and recycle grit, which were collected with plastic bags, were weighed. The two different working conditions produced the following results:

1. For concrete wall surface, we obtained 84.1% recycle grit from the dust of the existing separator (a total of 796.4g dust was fed to the new separator. We got 126.4g pure dust and 670.5g recycle grit.). The efficiency of the existing separator for this condition was 25%.

2. For coating on steel plate surface, we obtained 73.5% recycle grit from the dust of the existing separator (90.5g dust was fed to the new separator. We got 24.0g pure dust and 66.5g recycle grit.). The efficiency of the existing separator for this condition was 30%.

The above results prove the almost doubled efficiency and the improved separation efficiency to perfect status.

Similar to the blasting nozzle, the numerical simulation was carried out on the centrifugal separator again at the model test condition. Compared with the experimental result of this centrifugal separator, the difference between numerical and experimental results is below ±10% (75% from numerical modeling data for this case; 84.1% and 73.5% from experimental results mentioned above). Table 3 lists all the comparison results.

Table 3.
Comparison of the measurement results with CFD modeling data

	Efficiency (CFD modeling)	Efficiency (test data)	Deviation
Existing separator	27%	25% (for concrete surface)	5%
		20% (for coating on steel plate surface)	10%
Newly designed centrifugal separator	75%	84.1% (for concrete wall surface)	10%
		73.5% (for coating on steel plate surface)	5%

3.2.2 Velocity Distribution Test

In order to verify the modeling results, two different positions were chosen to obtain the new separator's internal velocity distribution. The experimental procedure was as follows.

Two ½ inch holes were drilled on the external surface of the separator. One is 2" and the other is 6" from the separator's top surface. The holes are on the opposite side surface of the separator's tangential air inlet channel. Two directional (tangential direction along the cylinder surface and axial along the vertical direction) velocities were measured to compare with the numerical simulation results. A 6060P Pitot probe from ALNOR INSTRUMENT COMPANY was employed to obtain the velocity distribution.

Figures 17 shows the results from one set of the experimental and numerical modeling tests Judging from these figures, the distinction of the experimental results and the estimated data agree very well with a deviation within ±10%. Therefore, it can be assumed that the numerical model and the newly designed separator are successful.

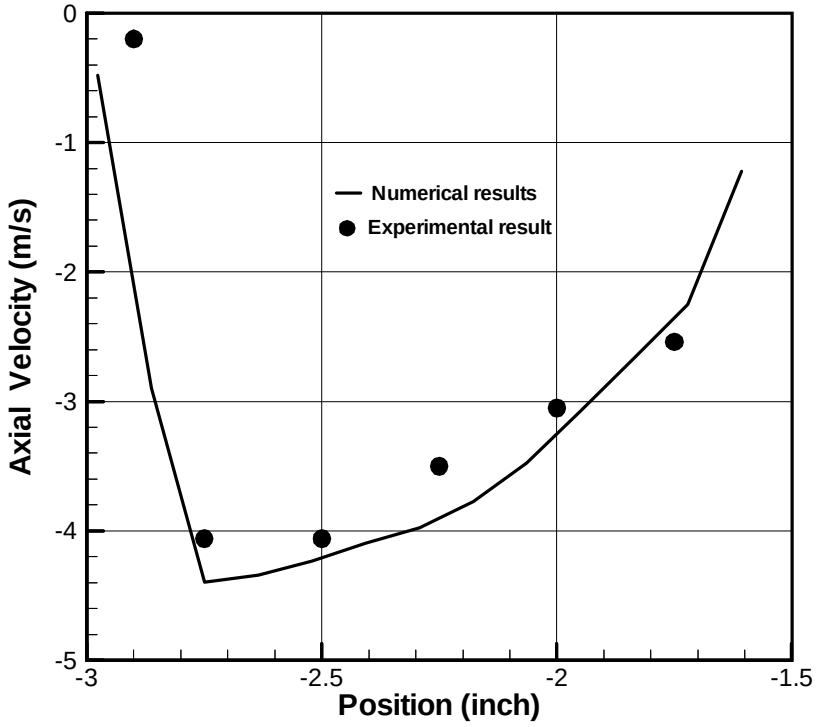

Figure 17. Comparison of numerical results and experiment data in the axial direction at the upper position (i.e., 2" to the separator's top surface).

CONCLUSION

Based on the test results, the goals established for Phase I of the project have been successfully fulfilled thereby providing a firm basis for the design The main conclusions are as follows:

- The numerical modeling of the blasting nozzles, including 1) circular and rectangular configuration; 2) the existing separator and newly designed centrifugal separator; and 3) the newly designed blasthead/wind curtain, have established configurations to meet the goals of the project.
- The designs of the rectangular blasting nozzle, new centrifugal separator, and blasthead/wind curtain have been completed, based on numerical modeling.
- An experimental system for to measure particle velocity speed and concentration and the separator efficiency has been set up using a high-speed video camera. These and other instruments, including pressure gauge, flow meter, thermocouples, and Pitot probe, have been employed in the experimental process.
- The fabrications of the blasting nozzle with ¼ inch equivalent throat diameter, collection box, centrifugal separator, and some other equipment were completed.
- The radiological characterization and lift-off sensor systems to be incorporated into the structure of the blasthead as compactly as possible, have been designed
- The model tests for nozzle and separator have been performed successfully. The comparisons of model test data for blasting nozzles and the new centrifugal separator have been completed demonstrating a maximum deviation from the experimental results for the modeling data is within ±10%. This proved that the mathematical models for simulating air-particle flow in the vacuum blasting system are successful.

The redesign of components based upon the above work is expected to enhance the productivity and economy of the vacuum blasting system by at least 50 percent over current vacuum blasting systems.